Anal Bioanal Chem (2016) 408:7271–7281
DOI 10.1007/s00216-016-9593-x

PAPER IN FOREFRONT

Improving impedimetric nucleic acid detection by using enzyme-decorated liposomes and nanostructured screen-printed electrodes

Diego Voccia[1] · **Francesca Bettazzi**[1] · **Emiliano Fratini**[1,2] · **Debora Berti**[1,2] · **Ilaria Palchetti**[1]

Received: 3 March 2016 / Revised: 10 April 2016 / Accepted: 20 April 2016 / Published online: 13 May 2016

Abstract Sensitive impedimetric detection of miR-222, a miRNA sequence found in many lung tumors, was investigated by using gold-nanostructured disposable carbon electrodes and enzyme-decorated liposomes. The proposed method was based on the immobilization of thiolated DNA capture probes onto gold-nanostructured carbon surfaces. Afterwards, the capture probes were allowed to hybridize to the target miRNAs. Finally, enzyme-decorated liposomes were used as labels to amplify the miRNA sensing, by their association with the probe–miRNA hybrids generated on the nanostructured transducer. By using this amplification route a limit of detection of 0.400 pM, a limit of quantification of 1.70 pM, and an assay range spanning three orders of magnitude (1.70–900 pM) were obtained (RSD % = 13). This limit of quantification was 20 times lower than that obtained using a simple enzyme conjugate for the detection. A comparison was also made with gold screen-printed transducers. In this case, a limit of quantification approximately 70 times lower was found by using the nanostructured transducers. Application of the optimized assay in serum samples was also demonstrated.

Published in the topical collection *Chemical Sensing Systems* with guest editors Maria Careri, Marco Giannetto, and Renato Seeber.

Electronic supplementary material The online version of this article (doi:10.1007/s00216-016-9593-x) contains supplementary material, which is available to authorized users.

✉ Ilaria Palchetti
ilaria.palchetti@unifi.it

[1] Dipartimento di Chimica, Università degli Studi di Firenze, Via della Lastruccia 3, Sesto Fiorentino 50019 Firenze, Italy

[2] CSGI, University of Florence, Via della Lastruccia 3, Sesto Fiorentino 50019 Firenze, Italy

Keywords Electrochemical impedance spectroscopy · Liposome · Alkaline phosphatase · Gold nanoparticles · Screen-printed electrodes

Introduction

Electrochemical impedance spectroscopy (EIS) is an interesting technique for the transduction of genosensing events at the surface of an electrode and many examples are reported in literature [1–3]. Its main advantage is that allows analysis of interfacial changes originating from hybridization events at the electrode surface in a "label-free" format [3, 4]. Nevertheless, to increase the sensitivity of the assay, amplified detection of the analyte DNA/RNA can be accomplished by the use of nanomaterials, by the catalytic activity of an enzyme, or by a combination of both. In particular, the use of enzyme labels, owing to their ability to convert single events (like hybridization) into a multitude of detectable molecules, has been extremely useful for the development of sensitive electrochemical bioaffinity assays.

In this paper, we describe an amplification strategy based on enzyme-decorated liposomes for the faradaic impedimetric detection of the hybridization reaction.

Liposomes are artificial vesicles, consisting of a phospholipid bilayer. In aqueous solutions, the hydrophilic head groups and the hydrophobic tails of the lipid molecules allow the liposomes to self-organize in spherical vesicles, in order to increase their solubility in the surrounding medium and minimize the surface-to-volume ratio. Phospholipids, which represent the main component of liposomes, possess different advantages like relatively low cost, biocompatibility, and lack of toxicity. The preparation of liposomes does not require tedious procedures or toxic reagents, and specific chemical moieties (e.g., biotin tag, functional groups, enzymes) can be

easily introduced [5, 6]. Thus, liposomes, with all the characteristics already mentioned, are versatile candidates for the development of biosensors. Despite these interesting features, only few examples of their use in the development of electrochemical genosensors have been reported so far [7]. Liposomes have insulating features due to their chemical composition [8], and electrochemical techniques, such as EIS, can be successfully used to measure the increase of the resistance to the electron transfer (R_{et}) at the electrode surface after liposome attachment. To the best of our knowledge, the use of liposomes as labels for the impedimetric detection of nucleic acids has been reported only by the Willner group [9–11]. In particular, liposomes modified with biotin and Horseradish Peroxidase (HRP) have been used for the sensing of model oligonucleotides, with a detection limit of 0.650 pM [9]. The biotin tag provided an anchoring site that links the biocatalytic liposome label to the biorecognition assembly. The enzyme HRP, incorporated in the liposome, stimulated the H_2O_2-biocatalyzed oxidation of 4-chloro-1-naphthol to form an insoluble product on the electrode surface that determined a further increase of R_{et} value measured by EIS [9].

In the present paper we investigated the use of alkaline phosphatase (AP)-decorated liposomes and the use of 5-bromo-4-chloro-3-indolyl phosphate (BCIP)/nitro blue tetrazolium (NBT) mixture [12] for the impedimetric detection of miRNAs via the biocatalyzed precipitation of an insoluble and insulating product onto the electrode surface. Biotin-conjugated nanosized liposomes were prepared and used as labels of the biotinylated hybrids formed on the electrode surface via streptavidin assembly. The biotin tags on the surface of the liposomes were then reacted with streptavidin–AP conjugate. Since one liposome can carry many enzyme molecules owing to its large surface area, the 1:1 enzyme-to-hybrid ratio is overcome with a magnification of the amplification event.

Moreover, as described in the literature [13], nanostructuring of the electrode surface is important to control the optimal distance among DNA capture probes at the electrode surface. Thus, we have optimized a procedure to electrodeposit gold nanoclusters to define nanoscale immobilization zones, where a few DNA strands are immobilized, thus limiting packing and consequently steric hindrance and electrostatic repulsion during the hybridization and labeling steps.

This enzyme-decorated liposome-based impedimetric genosensor has been applied for the detection of miRNAs in spiked human serum samples. Indeed, since their discovery in 1993 in the soil nematode *Caenorhabditis elegans* by the Ambros group [14], over the last decades miRNAs (microRNAs, miRs), a large class of small noncoding RNAs with approximately 20 nucleotides in length, have been considered to play important roles in different biological processes such as cell differentiation, proliferation, and regulation of protein translation. Abnormal miRNA expression (overexpression or downexpression) has been correlated with cancer and other diseases [15–17]. Tumor-derived miRNAs are present in human body fluids such as serum, plasma, urine, saliva, and sputum [18]. As a result of their tissue specificity and relative stability, circulating miRNAs offer great potential for use as minimally invasive diagnostic, prognostic, and predictive tumor biomarkers. Currently, different analytical methods can be used to detect miRNAs; each of these methods is characterized by its own unique advantages and disadvantages. Among them, quantitative reverse transcriptase polymerase chain reaction (qRT-PCR) is commonly used owing to the inherent sensitivity and reliability. However, the small size of miRNAs greatly complicates the use of PCR-based methods. Electrochemical genosensors have emerged as particularly attractive PCR-free options owing to their appropriate sensitivity, multiplexing capability, their simplicity to use, and the small amount of sample required [19–27].

Herein, the detection of miR-222, a miRNA sequence found in many lung tumors, has been demonstrated by using the newly developed impedimetric genosensor.

Materials and methods

Reagents

Streptavidin–alkaline phosphatase (S2890, Strept–AP, 2:1 conjugation stoichiometry), streptavidin (S4762, Strept), dithiothreitol (DTT), diethyl pyrocarbonate (DEPC), 6-mercapto-1-hexanol (MCH), 5-bromo-4-chloro-3-indolyl phosphate (BCIP), BCIP/nitro blue tetrazolium mixture [BCIP/NBT], Tris-HCl, bovine serum albumin (BSA), diethanolamine (DEA), dimyristoylphosphatidylethanolamine (DMPE), distearoylphosphatidyl choline (DSPC), cholesterol and human serum from AB plasma samples were obtained from Sigma–Aldrich (Milan, Italy). Biotin-XDHPE was obtained from Invitrogen Molecular Probes (Milan, Italy). Sulfuric acid, potassium hexacyanoferrate(III and II), disodium hydrogen phosphate, magnesium chloride, potassium chloride, and 4-(2-hydroxyethyl)-1-piperazineethanesulfonic acid sodium salt (HEPES) were purchased from Merck (Milan, Italy). NAP-10 columns of Sephadex G-25 were obtained from Amersham Pharmacia Biotech (Uppsala, Sweden). MilliQ water (DEPC treated for RNA analysis) was used throughout this work. Synthetic oligonucleotides were obtained from MWG Biotech AG (Germany):

Capture probe (CP): 5′ GAA-ACC-CAG-CAG-ACA-ATG-TAG-CT–SH 3′

Target miR-222: 5′ AGC-UAC-AUC-UGG-CUA-CUG-GGU-CUC–biotin 3′

Non-complementary miR-16: 5′ UAG-CAG-CAC-GUA-AAU-A–biotin 3′

Prior to use, the thiol-modified oligonucleotides (CP) were treated with DTT. This reagent allowed reduction and

cleavage of oligo dimers produced by oxidative coupling of two DNA-SH molecules (i.e., DNA-S-S-DNA). The lyophilized oligonucleotides were dissolved in a 10 mM Tris-HCl buffer solution (pH 8.3) containing 20 mM of DTT. The reaction was allowed to proceed for 2 h at room temperature. The CPs were then purified by elution through a NAP-10 column of Sephadex G-25 using 0.5 M phosphate buffer (pH 7.0). CP stock solutions were stored frozen.

Buffer solutions, if not otherwise stated, were (a) phosphate buffer (PB) comprising 35.6 % KH_2PO_4 and 64.4 % Na_2HPO_4 (0.5 M, pH 7.0); (b) diethanolamine (DEA) comprising 0.1 M diethanolamine pH 9.6, 0.1 M KCl, 1 mM $MgCl_2$.

All chemicals used in this study were analytical reagent grade.

Preparation of liposomes

Liposomes containing DSPC/cholesterol/DMPE/DHPEX-biotin in a molar ratio 40:40:19.5:0.5 were prepared by extrusion through polycarbonate membranes as described by Alfonta et al. [9]. Extrusion was carried out using a manual liposome extruder (LiposoFast-Basic, Avestin Inc., Canada). The dry lipids were dispersed in 20 mM HEPES, pH 7.4, 0.15 M NaCl with vortex mixing. The solution containing the mixture was passed 20 times through a polycarbonate membrane of 100 nm pore size and 19 mm diameter (Avestin Inc., Canada), by pushing the sample back and forth between two syringes. The liposome dispersion was stored at 4 °C, until further use.

Characterization of liposomes

Dynamic light scattering (DLS) was used to evaluate the hydrodynamic diameters of liposomes using a Zetasizer Nano ZS90 system (Malvern). Samples for size measurement were prepared by addition of 25 μL of liposome dispersion to 2 mL of 10 mM PB, pH 7.4. Prior to use, the solution was filtered using a 0.2 μm syringe filter and dispensed into a clean plastic cuvette. To confirm the presence of biotin on the surface of liposomes, hydrodynamic diameters of liposome aggregates were estimated by DLS using a Brookhaven Instruments apparatus (BI9000AT correlator card and BI200SM goniometer). The light source was the second harmonic of a diode-pumped Coherent Innova Nd:YAG laser (λ = 532 nm). The signal was detected by an EMI 9863B/350 photomultiplier. To obtain the size distribution of the scattering objects, the autocorrelation functions were Laplace inverted using the CONTIN routine. Samples for the aggregation test were prepared by addition of 25 μL of a 1:1 mixture of liposomes and streptavidin (0.5 mg/L in PB), which was incubated in a vial for 20 min under mixing, to 2 mL of 10 mM phosphate buffer, pH 7.4. A sample with only liposomes was used as negative control. The solution was filtered using a 0.2 μm syringe filter and dispensed into a clean glass cuvette.

Electrodes

The electrochemical cell consisted of a planar, screen-printed, three-electrode strip based on a carbon (SPCE) or gold (SPGE) working electrode (3 mm diameter, geometrical area 7 mm^2), a carbon counter electrode, and a silver pseudo-reference electrode. Materials and procedures to screen-print the electrodes were described in previously published papers [28–31].

Prior to immobilization of the CPs, carbon working electrodes were modified by potential-sweeping electrodeposition of Au from 1 mM $HAuCl_4 \cdot 3H_2O$ in 0.01 M Na_2SO_4 and 0.01 M H_2SO_4 solution, through cyclic voltammetry (CV) with the following parameters: scan rate 50 mV/s, cathodic switching potential −0.6 V, and anodic switching potential +1.5 V. Gold-modified SPCE were denominated Au-SPCE.

Furthermore, CV scans in 0.5 M H_2SO_4 were performed to characterize the modified electrode. The recorded charge under the reduction peak was used for the characterization of the electroactive electrode area, assuming 482 μC cm^{-2} to be the charge required for the reduction of a monolayer of oxides on polycrystalline gold electrodes [32] and calculating the area of the peak at +0.76 V.

Furthermore, the electrochemically active surface of the Au-SPCEs was also evaluated by CV in the presence of the 5 mM ferrocyanide in 0.1 M KCl. The Randles–Sevcik equation was used:

$$i_p = \left(2.687 \times 10^5\right) n^{3/2} A D^{1/2} C \nu^{1/2}$$

where i_p is the ferrocyanide peak current, n the number of electrons involved, A the electrode area (cm^2), D the diffusion coefficient (=6.50×10^{-6} cm^2/s) C the concentration (mol/cm^3), and ν the scan rate (V/s).

Electrochemical measurements

Electrochemical experiments were conducted with an AUTOLAB PGSTAT 10 digital potentiostat/galvanostat controlled by GPES 4.9004 software (Eco Chemie BV, Utrecht, the Netherlands). All potentials reported in this work were referred to the silver pseudo-reference electrode; the experiments were performed at room temperature, without deoxygenation.

EIS tests were carried out in 0.1 M KCl containing 5 mM of $K_3Fe(CN)_6$ and 5 mM of $K_4Fe(CN)_6$ (redox probe solution). Seventy microliters of the redox probe solution was casted onto the planar sensor surface, covering the counter, working, and pseudo-reference electrodes.

A frequency range from 100 kHz to 10 mHz with a sinusoidal voltage of 10 mV and a bias potential of +0.13 V was used. The data, presented in the form of complex plane diagrams (i.e., Nyquist plots), were fitted with a proper equivalent circuit (modified Randles circuit) using FRA2 software 4.9004 (EcoChemie). Both electron transfer resistance (R_{et}) and delta electron transfer resistance values (i.e., $\Delta R_{et} = R_{et} - R_{et\ blank}$) were evaluated as analytical signal.

SEM-EDX characterization

Scanning electron microscopy (SEM) was performed on uncoated samples using a ΣIGMA field emission scanning microscope (Carl Zeiss Microscopy GmbH, Germany). High resolution images were acquired with an acceleration potential of 2 kV and a working distance of about 1.5 mm using the Inlens high resolution secondary electron detector. Qualitative compositional images were obtained using a retractable back scattering detector (BSD), working at a distance of 8 mm with an acceleration potential of 9 kV. The SEM micrographs were analyzed with Image J software (http://imagej.nih.gov/ij/) to obtain information about the particle size distribution. Chemical elements contained in the matrix were determined using energy-dispersive X-ray spectroscopy (EDX) that was performed by using a 10 mm^2 silicon drift detector (X-Act) coupled with the SEM microscope operated by the INCA software (Oxford Instruments, UK). In this case, the operative voltage of the electron source was about 9 kV and the working distance was 8.5 mm to maximize the X-ray photon counts. Prior to SEM imaging, samples were thoroughly rinsed with Milli-Q water and dried under reduced pressure in a vacuum desiccator with a standard membrane pump for a few hours.

Probe immobilization

CP immobilization was accomplished by applying 10 μL of the CP solution (2 μM in PB) onto the Au-SPCE working electrode surface in a moisture-saturated environment chamber, overnight (≈16 h). The CP-coated surface was subsequently treated with MCH (spacer thiol). Ten microliters of 1 mM aqueous solution of MCH was placed onto the CP-modified surfaces for 1 h. Afterwards, the modified electrodes were treated twice with 30 μL of PB.

Hybridization procedure

Hybridization experiments were performed in a direct format. Ten microliters of the biotinylated target sequence solution (in 0.5 M PB) was placed onto CP-modified Au-SPCE. After 20 min (hybridization time), the sensors were washed twice with 30 μL of DEA buffer in the case of the strept–AP assay or with 0.1 M PB, pH 7.4, in the biotin-tagged liposome assay scheme. As negative control, a biotinylated non-complementary sequence was used.

Labeling and EIS detection

Strept–AP-based assay The biotinylated hybrid was reacted with 10 μL of a solution containing 0.8 U/mL of strept–AP conjugate and 10 mg/mL of BSA (as blocking agent) in DEA buffer for 20 min. After a washing step (30 μL of DEA buffer for two times), the enzyme-modified surfaces were exposed to 30 μL of the BCIP/NBT mixture for 20 min. Afterwards, the sensors were washed with 0.1 M KCl.

Enzyme-decorated liposome assay The biotinylated hybrid obtained at the electrode surface was reacted with a 10 μL solution containing 0.05 mg/L of streptavidin in PB for 20 min. Afterwards, the genosensor was washed twice with 30 μL of HEPES buffer and then reacted with liposome dispersion (20 min, room temperature). Then, after a washing step with DEA buffer, a solution containing 10 μL of 0.8 U/mL strept–AP conjugate and 10 mg/mL BSA in DEA buffer was added for 20 min. The enzyme–liposome-modified surfaces were cleaned with 30 μL of DEA buffer and then incubated with 30 μL of the BCIP/NBT mixture for 20 min. During incubation, an insoluble and insulating product precipitated onto the surface. Finally, the genosensor was examined by EIS (in the presence of the redox probe solution), having been previously cleaned with 0.1 M KCl.

Each result is the mean and standard deviation of at least three measurements.

Calibration plot

The calibration plot was fitted by non-linear regression to the four-parameter logistic (4-PL) equation using Origin Pro 2015 software (Origin Lab Corporation, USA) according to the following formula:

$$Y = A + \frac{(B - A)}{1 + \left(x / C\right)^{m}}$$

in which Y is the analytical signal, A is the analytical signal at infinite analyte concentration, B is the analytical signal at zero analyte concentration, x is the analyte concentration, C is the inflection point on the calibration curve (the analyte concentration necessary to have 50 % of the signal), and m is the slope of the linear part of the curve [33, 34].

The limit of detection (LOD) value was evaluated considering the average response of the blank plus three times the standard deviation, whereas the limit of quantification (LOQ) was estimated considering the average response of the blank plus 10 times the standard deviation. The obtained values

were converted into moles per liter by fitting the data to the calibration function.

The upper limit of quantification (ULOQ) was considered as the highest amount of an analyte in a sample that can be quantitatively determined with precision and accuracy; it was assessed as the concentration corresponding to 90 % of the maximum signal, with an acceptable RSD % ≤ 20 % ($n = 3$).

The quantification range was considered to be the range of concentration (including ULOQ and LOQ) that can be reliably and reproducibly quantified with accuracy and precision through the use of a concentration–response relationship.

Human serum spiked samples

Human serum type AB was diluted 1:100 (v/v) in PB and filtered (0.45 μm). Spiked samples were prepared by adding known quantities of miR-222 to diluted serum.

Results and discussion

Development of the impedimetric assay

The proposed assay was based on Au-nanostructured, screen-printed carbon electrodes and on enzyme-decorated lyposomes (Scheme 1). The first step of the assay consisted of the electrodeposition of Au nanoclusters on the surface of a bare SPCE. These Au nanoclusters offered an excellent platform to immobilize the DNA capture probes (CP) via Au–thiol chemisorption. Then, MCH was introduced onto the electrode surface to eliminate the possible remaining active groups and to block the nonspecific binding sites. The CP-modified electrode was then allowed to react with the analyte (the target miRNA). Then, streptavidin and biotinylated liposomes were sequentially added. Afterwards, the liposome-modified hybrid was exposed to strept–AP. The high surface-to-volume ratio of the liposome offers a reliable support for enzyme immobilization, thus allowing for the simultaneous presence of a multitude of enzyme molecules per hybrid formed on the electrode surface. After incubation of the substrate, the enzymatic product was revealed by faradaic EIS, in the presence of $[Fe(CN)_6]^{3/4-}$.

Liposome characterization, in terms of dimensions, conjugation to streptavidin, and stability, as well as the electrochemical, SEM, and EDX characterization of the nanostructured surface is reported in the following paragraphs.

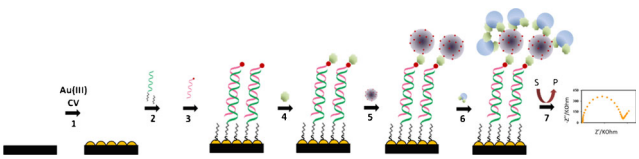

Scheme 1 Assay scheme. (*1*) Gold nanoclusters were electrochemically deposited by reduction of 1 mM $HAuCl_4$ solution at the SPCE surface, using cyclic voltammetry (CV). The DNA CP was immobilized on the nanostructured surface (*2*). The CP-modified Au-SPCE, backfilled with mercaptohexanol (*2*), was exposed to the target miRNA (*3*). The biotinylated hybrid is formed on the Au-SPCE surface. Streptavidin (*4*) and biotinylated liposomes (*5*) are sequentially added. The liposome-modified hybrid is then exposed to streptavidin–alkaline phosphatase (*6*). After incubation of the substrate, the enzymatic product is revealed by EIS (*7*)

Liposome characterization

The hydrodynamic diameter (146 ± 9 nm) of the biotinylated liposomes was evaluated by DLS and controlled by choosing appropriate extrusion membranes, as described in the "Materials and methods" section. The size distribution of the biotinylated liposomes was determined on the same day as their preparation and compared with those stored for 1 month at 4 °C (stability test). Aggregation of liposomes during the stability test was negligible (data not shown).

The presence of the biotin tags on the surface of the liposomes was also evaluated by DLS by monitoring the increase of the hydrodynamic diameter after the addition of a known concentration of streptavidin (0.5 mg/L) in the dispersion of the biotinylated liposomes (see Electronic Supplementary Material (ESM) Fig. S1). As a result of the four biotin-binding sites, streptavidin acted as a biological cross-linking agent and initiated the formation of liposome aggregates with an increase of the average size. The hydrodynamic diameter of the liposome population increased in the presence of the streptavidin from 140 to 250 nm, confirming the interaction of streptavidin with the biotinylated liposomes. However, the size distribution of the aggregates suggested that only a small fraction of the biotin binding sites of streptavidin was available to biotinylated liposomes. The size of the streptavidin molecule (5–6 nm) was small compared with the size of the liposomes; thus, surface geometry prevented binding of liposomes to more than one or two sites on streptavidin. Nevertheless, the DLS analysis confirmed the availability of biotin moiety at the liposome external surface.

Au electrodeposition and electrochemical characterization of the nanostructured surfaces

Au nanoclusters were electrochemically deposited by reduction of 1 mM $HAuCl_4$ solution at the SPCE surface using CV. As reported in Fig. 1, on the negative sweep of the first CV scan cycle, a broad reduction peak (+0.16 V), indicating the reduction of Au(III) to Au(0), was observed. Moreover, a current crossover on the reverse scan was present. This crossover, indicative of nucleation growth kinetics, was followed by a large anodic process (near +0.90 V) due to both the formation of an oxide layer on the electrodeposited gold and electrodissolution of Au(0) [35]. On the second potential scan

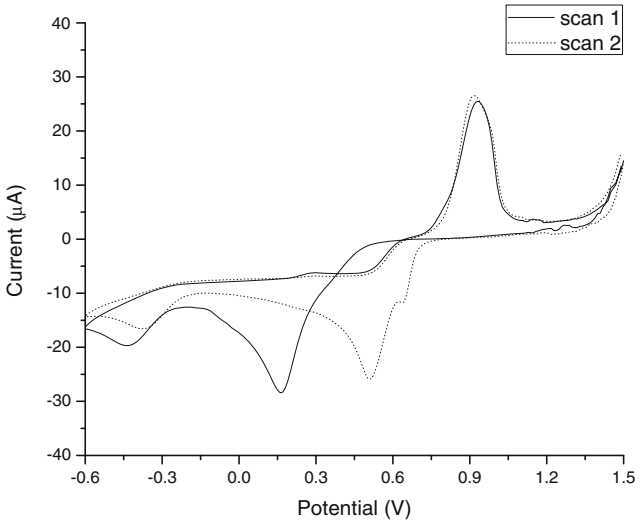

Fig. 1 Cyclic voltammetry obtained at an SPCE electrode in 1 mM $HAuCl_4$, 0.01 M Na_2SO_4, and 0.01 M H_2SO_4 solution. Potential scan, from +1.5 to −0.6 V; step potential, 2.44 mV; scan rate, 50 mV/s

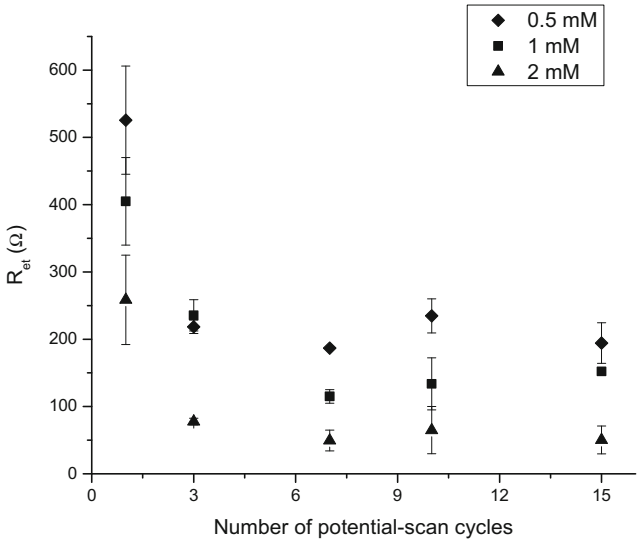

Fig. 2 Electron transfer resistance (R_{et}) values at the Au-SPCE after varying the potential scan cycle number (1, 3, 7, 10, 15) and Au(III) concentration (0.5, 1, and 2 mM). All other experimental conditions for the electrode modification are the same as reported in Fig. 1. Each *point* represents the mean of at least three measurements and the *error bars* the corresponding standard deviation

cycle, a large positive shift (from +0.16 to +0.51 V) in the Au(III) reduction peak, due to nucleation sites created on the first scan, was found. The cathodic peak at +0.64 V was due to the reduction of gold oxide formed in the first scan. In addition, no current crossover was observed. The shapes of these voltammograms were consistent with those previously described under similar conditions [35–37].

To optimize the electrodeposition process, the effect of the concentration of $HAuCl_4$ and the number of potential scan cycles were evaluated. As reported in the literature, these parameters play an important role for the morphology, size, and uniformity of particles [36].

Figure 2 shows the influence of these variables by analyzing, after each electrodeposition scan, the values of the electron transfer resistance (R_{et}) of a redox probe, measured by EIS. Thus, the electrode was rinsed with deionized water and then 100 μL of 5 mM $[Fe(CN)_6]^{3/4-}$ (1:1 mixture in 0.1 M KCl) was casted onto the sensor surface and the impedance spectra recorded. As reported in Fig. 2, a progressive reduction in the R_{et} value was observed on increasing both the variables. This is consistent to the fact that a higher electrode surface area was coated with Au nanoclusters [38].

The number of potential scan cycles was varied from 1 to 15. R_{et} decreased with increasing number of cycles (Fig. 2), reaching a constant value after 7 cycles (133 ± 19 Ω). Thus, the number of potential scan cycles for the electrodeposition of gold nanoclusters for further experiments was determined to be 7.

The $HAuCl_4$ concentration was varied in the range 0.5–2.0 mM, obtaining a decrease of R_{et} with increasing Au(III) concentration (Fig. 2).

However, as reported in the literature [36], the most homogenous deposits were obtained using low Au(III) concentrations. These data were also confirmed by SEM morphological studies (Fig. 3). For this reason, 1 mM $HAuCl_4$ concentration was chosen as a compromise between R_{et} value and morphology of the surface.

The nanostructured electrodes were then characterized by performing CV scans in 0.5 M H_2SO_4 (ESM Fig. S2a). The presence of oxidation and reduction peaks typical of gold were observed [35, 39]. The recorded charge under the reduction peak was used for the characterization of the electroactive electrode area [32]. An electrochemically active area of 4.9 ± 0.2 mm^2 was estimated, in contrast to a geometrical area of 7.1 mm^2.

Furthermore, the electrochemically active area was also evaluated by CV in the presence of 5 mM ferrocyanide in 0.1 M KCl (ESM Fig. S2b). Using the Randles–Sevcik equation, as reported in the "Materials and methods", we determined the electrochemically active surface to be 4.7 ± 0.2 mm^2. This value was in good agreement with that previously described.

The standard deviation of these measurements indicated the good reproducibility of the gold electrodeposition process.

Surface characterization using SEM and EDX

Information on the shape and size of Au nanoclusters was obtained by SEM observations. Figure 3 shows typical SEM micrographs of the bare SPCE (Fig. 3a, d) and of the Au-SPCE (electrodeposited from 1 mM Au(III) solution (Fig. 3b, e) and from 2 mM Au(III) solution (Fig. 3c, f),

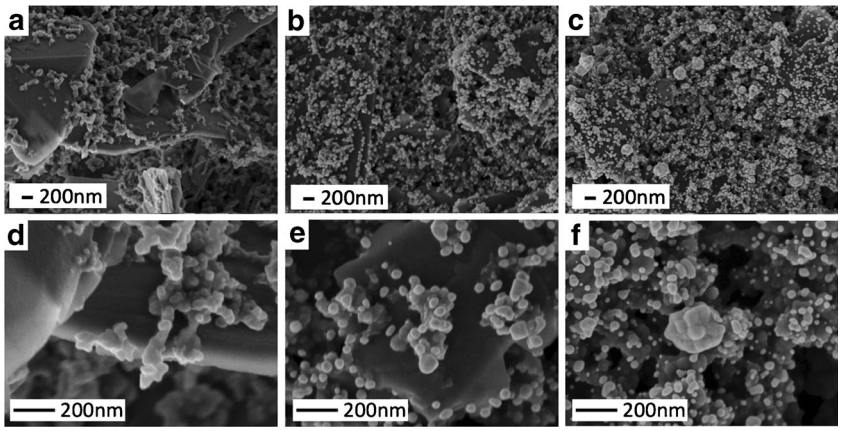

Fig. 3 SEM images of a bare SPCE (**a**, **d**), with typical roughness and nanostrucuration of the carbon electrode surface; 1 mM gold-modified SPCE (**b**, **e**); 2 mM gold-modified SPCE (**c**, **f**). All samples are prepared in experimental conditions as reported in the text using InLens detector

respectively). The SEM images confirm the formation of nanosized Au clusters with an average diameter of 55 ± 15 nm (with a density of 77 particles per μm^2) and 168 ± 100 nm (with a density of 145 particles per μm^2) on the carbon surface, for 1 mM Au(III) and 2 mM Au(III)-modified electrodes, respectively. Thus, an increase in the particle density and in average size as a function of the Au(III) concentration was observed (Fig. 3b, e and c, f), illustrating a gradual coalescence phenomenon [36]. Distribution analysis is reported in Fig. S3 in the ESM, confirming the presence of two distinct populations for 2 mM Au(III)-modified electrodes: the first one is related to small and spherical-shaped nanoparticles (NPs) and the second one to larger, aggregate-like NPs. Au deposits were absent in the negative control, even if SEM micrographs showed nanostructures likely due to carbon screen-printing ink composition.

Qualitative compositional images, obtained using BSD and reported in Fig. 4, clearly demonstrated the differences between the SPCE (4a) and the Au-SPCE (4b) surface.

Electrode surface elemental analysis by EDX was also performed and the results are reported in Table 1. The results confirm that the main components of the Au-SPCE electrode surface are C and Au, with traces of chloride and oxygen. The presence of O and Cl elements is due to the screen-printing ink composition, according to the information provided by the manufacturer. In particular, the chlorine peak is due to the presence of vinyl chloride and acrylate copolymer, the binders used in the printing process.

Optimization of surface coverage and other assay parameters

The impedimetric spectra upon the different steps of the assay, according to Scheme 1, are shown in Fig. 5. The interaction of target microRNA with the sensing interface (CP/MCH) to form the hybrid via base-pairing resulted in an increase in the electron transfer resistance at the electrode (R_{et} = 1.2 ± 0.2 kΩ). The association of streptavidin also raised the value of the interfacial electron transfer resistance, as a result of the partial hydrophobic insulation of the electrode surface. The association of the biotin-functionalized liposome further increased R_{et} to 3.0 ± 0.3 kΩ. Finally, the insoluble product of the enzymatic reaction led to a significantly higher value of R_{et} (6.3 ± 0.7 kΩ).

Indeed, the amplification of the analytical signal was the result of two main factors: (i) lyposomes, as a result to their chemical composition, acted as insulating systems of the electrode surface. Thus, the interfacial electron transfer process was perturbated and the R_{et} value increased; (ii) as a result of the precipitation of the insoluble product because of the hybridization reaction and the enzymatic biocatalytic activity, the accumulation of an insulating layer on the electrode further increased R_{et}.

The amount of the target miRNA hybridized on the electrode surface controlled the amount of liposomes associated with the electrode. The content of the enzyme molecules associated with the sensing interface as well as the time interval

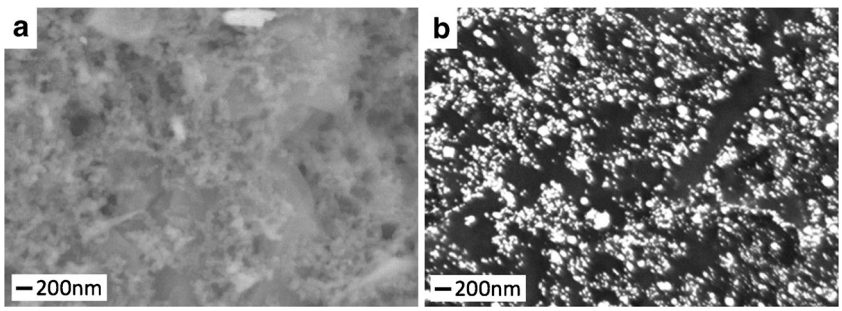

Fig. 4 SEM images of bare (**a**) and 1 mM gold-modified (**b**) screen-printed carbon electrode prepared in experimental conditions as reported in the text using a BSD detector; the primary contrast mechanism is due to differences in atomic number (*Z*) so that areas of the sample with heavier elements appear brighter

Table 1 EDX analysis of elements of 666 μm^2 electrode area of different types of electrodes

	SPCE[a]	1 mM Au-SPCE[a]	2 mM Au-SPCE[a]
C	96.2	96.2	95.3
O	2.5	2.1	1.9
Cl	1.4	1.0	1.6
Au	–	0.7	1.2

Reported values correspond to Atomic %

[a] Unmodified carbon electrode (SPCE), gold-modified carbon electrode with 1 mM Au(III) solution (1 mM Au-SPCE), and gold-modified carbon electrode with 2 mM Au(III) solution (2 mM Au-SPCE)

employed for the biocatalyzed precipitation process controlled the amount of precipitate that was accumulated on the electrode. All the parameters that may affect the performance of the assay were optimized, as shown in Table S1 in the ESM. One of the parameters that was finely controlled was the CP concentration during genosensor fabrication. As highlighted in the literature [40], CP density can be experimentally controlled by changing the CP concentration. Electrode surfaces characterized by lower CP density show a reduced number of biorecognition sites, whereas surfaces with higher CP densities can cause steric and electrostatic interference between packed probes and the incoming target and liposomes. Higher analytical signal was obtained with electrodes modified with 2 μM of the CP solution and therefore this concentration was used for further measurements.

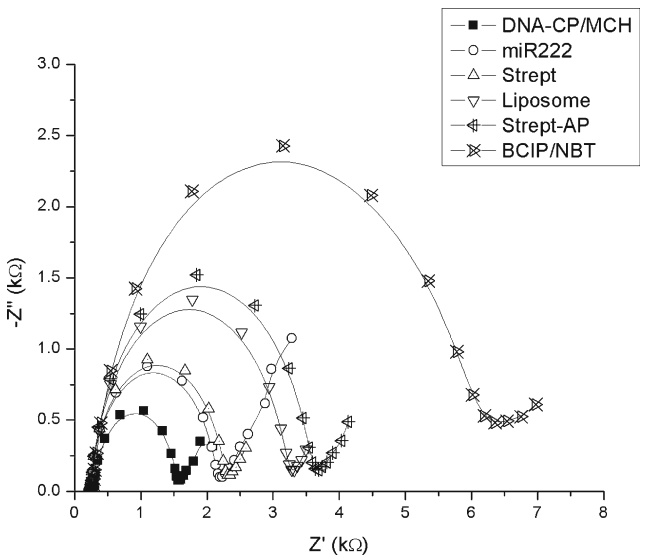

Fig. 5 Faradaic impedance spectra (in the form of Nyquist plots) for the measurements corresponding to (1) probe functionalized electrode; (2) after interaction with 0.1 nM miRNA target; (3) after treatment with streptavidin; (4) after interaction with liposomes; (5) after interaction with strept–AP; (6) after interaction with the substrate. Data are recorded in 0.1 M KCl in the presence of $[Fe(CN)_6]^{3/4-}$ (5 mM, 1:1). Further details are reported in the text

Analytical evaluation of the assay

A calibration experiment was designed to demonstrate the analytical performances of the impedimetric assay. The 4PL equation was used to fit the data ($R^2 > 0.99$). The limit of detection was evaluated to be 0.400 pM (i.e., 4 amol in 10 μL of sample solution) using the criterion of the background signal plus three times its standard deviation. The response of the assay spanned over three orders of magnitude, with a limit of quantification (defined as the background signal plus ten times its standard deviation) of 1.70 pM. The upper limit of quantification was 900 pM, with an RSD % = 13 % ($n = 3$) between a target concentration of 0 and 900 pM. A typical calibration curve is shown in Fig. 6.

Non-complementary sequence solutions at concentrations of 10, 100, and 1000 nM were also analyzed. All the concentrations tested produced a similar value of ΔR_{et} (0.15 ± 0.04 kΩ), demonstrating that the non-complementary sequence did not interact nonspecifically with the transducer surface and had no cross-reactivity with the immobilized CPs.

The analytical performances of the assay were evaluated in comparison with results obtained using strept–AP conjugate as a label, as well as the data obtained using an SPGE.

Table 2 reports the improved analytical performances of the proposed assay over other assays based on the use of strept–AP (instead of enzyme-decorated liposomes) or on the use SPGEs (instead of nanostructured transducers). In the first approach we were interested to study the effect of the liposomes as

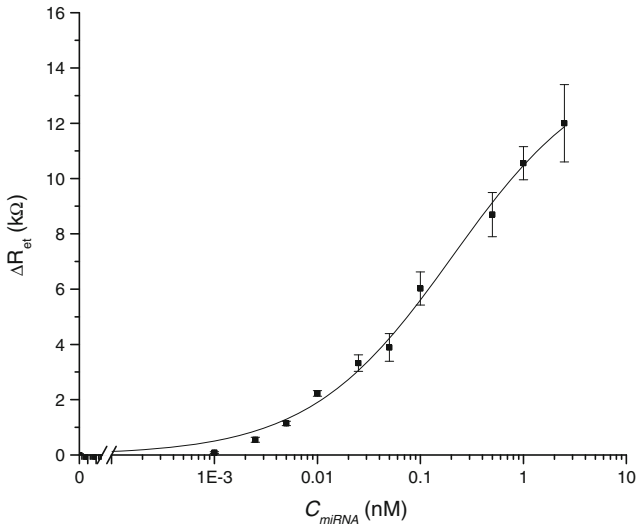

Fig. 6 miR-222 calibration plot in PB. Further details are available in the "Materials and methods" section. Each *point* represents the mean of at least three measurements and the *error bars* the corresponding standard deviation

Table 2 Comparison of the analytical performances of the different assays

Electrode	Label	Dynamic range (nM)	R^2	LOD (pM)	LOQ (pM)	ULOQ (pM)	RSD (%)
SPGE[a]	Lip	0.01–1	0.99	40	117	700	15
Au-SPCE[b]	Strept–AP	0.01–1	0.99	10	35	500	18
Au-SPCE[c]	Lip	0.001–1	0.99	0.4	1.7	900	13

[a] SPGEs used as transducers and enzyme-decorated liposomes as labels

[b] Au-SPCEs used as transducers and strep-AP as labels

[c] Au-SPCEs used as transducer and enzyme-decorated liposomes as labels

nanoarchitectures rich in enzymatic labels with respect to the 1:1 enzyme-to-hybrid ratio. Whereas, in the other approach, we were interested to evaluate the effect of the Au-nanostructuring with respect to the use of a planar gold screen-printed electrode.

When compared to detection with strept–AP (Table 2), the enzyme-decorated liposomes showed better performance in the lower end of the concentration range. The limit of detection of the strept–AP assay was 10 pM and the limit of quantification was 35 pM. These results confirm the magnification of the enzyme-mediated biocatalytic reaction attributed to each liposome being able to bind many enzyme molecules per hybridization event.

In addition, the performances of the nanostructured surface were also compared with those of SPGE using the same CPs and enzyme-decorated lyposomes. The limit of quantification was a factor of 70 lower for the nanostructured electrode than for gold electrodes. The better analytical performances of the proposed assay were attributed to higher level of DNA probe immobilization and to the improved conditions for effective surface hybridization between the CP and the target as a result of surface nanostructuring.

Application: analysis in serum

The reliability and feasibility potential of using this impedimetric genosensor for clinical analysis were also assessed. Thus, a series of samples were prepared by adding different concentrations (10, 50, 100, and 500 pM) of miR-222 to diluted human blood serum samples. As shown in Table 3, the recovery was between 77 % and 93 %. A suppression of the analytical signal in the presence of the matrix was generally observed. From these values, the enzyme-decorated liposome assay seemed a feasible method for determining miR-222 in real biological samples.

Table 3 Recovery of the proposed miRNA assay in human serum samples

Sample no.	Found (pM)	Spiked (pM)	Recovery
1	9.3 ± 0.4	10	93
2	38 ± 3	50	77
3	88 ± 3	100	88
4	400 ± 1	500	80

Conclusions

In this work, we have demonstrated the improvement in the analytical performances of an impedimetric genosensor by using enzyme-decorated liposomes and nanostructured electrodes.

We have demonstrated the benefit of enzyme-decorated liposomes over streptavidin–alkaline phosphatase conjugate as labeling reagent for hybridization detection. The high surface-to-volume ratio of the liposome offers a reliable support for enzyme immobilization, thus allowing for the simultaneous presence of a multitude of enzyme molecules per hybrid formed on the electrode surface. The nanostructuring of the electrode surface offers suitable immobilization sites for the capture probes, thereby allowing optimal control over steric hindrance.

A comparison was made with gold electrodes for CP immobilization and strept–AP for detection, which yielded a limit of quantification approximately 70 and 20 times higher than that for nanostructured electrodes and enzyme-decorated liposomes, respectively.

This method was also well suited for the detection of miRNA sequences in serum samples. A small RNA can be quite easily terminal conjugated with biotin, and a procedure to label miR-222 with biotin was recently reported [30]. This procedure should be further implemented and optimized to analyze miRNAs in serum samples

Acknowledgments This work was supported by Ministero dell'Istruzione, dell'Università e della Ricerca (MIUR) in the framework of Progetti di ricerca di interesse nazionale (PRIN) 2012 (grant no. 20128ZZS2H) and Ente Cassa di Risparmio di Firenze project ID PED 8780 2014.0757A2202.0734.

EF and DB acknowledge CSGI (Consorzio per lo Sviluppo dei Sistemi a Grande Interfase) for partial financial support.

Compliance with ethical standards

Conflict of interest No conflict of interest is declared.

References

1. Suni II. Impedance methods for electrochemical sensors using nanomaterials. TrAC Trends Anal Chem. 2008;27:604–11. doi:10.1016/j.trac.2008.03.012.
2. Katz E, Willner I. Probing biomolecular interactions at conductive and semiconductive surfaces by impedance spectroscopy: routes to impedimetric immunosensors, DNA-sensors, and enzyme biosensors. Electroanalysis. 2003;15:913–47. doi:10.1002/elan.200390114.
3. Daniels JS, Pourmand N. Label-free impedance biosensors: opportunities and challenges. Electroanalysis. 2007;19:1239–57. doi:10.1002/elan.200603855.
4. Labuda J, Oliveira Brett AM, Evtugyn G, Fojta M, Mascini M, Ozsoz M, et al. Electrochemical nucleic acid-based biosensors: concepts, terms, and methodology (IUPAC Technical Report). Pure Appl Chem. 2010;82:1161. doi:10.1351/PAC-REP-09-08-16.
5. Edwards KA, Baeumner AJ. Optimization of DNA-tagged dye-encapsulating liposomes for lateral-flow assays based on sandwich hybridization. Anal Bioanal Chem. 2006;386:1335–43. doi:10.1007/s00216-006-0705-x.
6. Edwards KA, Curtis KL, Sailor JL, Baeumner AJ. Universal liposomes: preparation and usage for the detection of mRNA. Anal Bioanal Chem. 2008;391:1689–702. doi:10.1007/s00216-008-1992-1.
7. Chumbimuni-Torres KY, Wu J, Clawson C, Galik M, Walter A, Flechsig G-U, et al. Amplified potentiometric transduction of DNA hybridization using ion-loaded liposomes. Analyst. 2010;135:1618–23. doi:10.1039/C0AN00198H.
8. Kannuck RM, Bellama JM, Durst RA. Measurement of liposome-released ferrocyanide by a dual-function polymer modified electrode. Anal Chem. 1988;60:142–7. doi:10.1021/ac00153a009.
9. Alfonta L, Singh AK, Willner I. Liposomes labeled with biotin and horseradish peroxidase: a probe for the enhanced amplification of antigen − antibody or oligonucleotide − DNA sensing processes by the precipitation of an insoluble product on electrodes. Anal Chem. 2001;73:91–102. doi:10.1021/ac000819v.
10. Patolsky F, Lichtenstein A, Willner I. Electronic transduction of DNA sensing processes on surfaces: amplification of DNA detection and analysis of single-base mismatches by tagged liposomes. J Am Chem Soc. 2001;123:5194–205. doi:10.1021/ja0036256.
11. Patolsky F, Lichtenstein A, Willner I. Electrochemical transduction of liposome-amplified DNA sensing. Angew Chem Int Ed. 2000;39:940–3. doi:10.1002/(SICI)1521-3773(20000303)39:5<940::AID-ANIE940>3.0.CO;2-Y.
12. Palchetti I, Laschi S, Marrazza G, Mascini M. Electrochemical imaging of localized sandwich DNA hybridization using scanning electrochemical microscopy. Anal Chem. 2007;79:7206–13. doi:10.1021/ac070474h.
13. Soreta TR, Henry OYF, O'Sullivan CK. Electrode surface nanostructuring via nanoparticle electronucleation for signal enhancement in electrochemical genosensors. Biosens Bioelectron. 2011;26:3962–6. doi:10.1016/j.bios.2011.03.001.
14. Lee RC, Feinbaum RL, Ambros V. The C. elegans heterochronic gene lin-4 encodes small RNAs with antisense complementarity to lin-14. Cell. 1993;75:843–54. doi:10.1016/0092-8674(93)90529-Y.
15. Calin GA, Croce CM. MicroRNA signatures in human cancers. Nat Rev Cancer. 2006;6:857–66.
16. Calin GA, Dumitru CD, Shimizu M, Bichi R, Zupo S, Noch E, et al. Frequent deletions and down-regulation of micro-RNA genes miR15 and miR16 at 13q14 in chronic lymphocytic leukemia. Proc Natl Acad Sci. 2002;99:15524–9. doi:10.1073/pnas.242606799.
17. Satoh J. Molecular network of microRNA targets in Alzheimer's disease brains. Exp Neurol. 2012;235:436–46. doi:10.1016/j.expneurol.2011.09.003.
18. Kosaka N, Iguchi H, Ochiya T. Circulating microRNA in body fluid: a new potential biomarker for cancer diagnosis and prognosis. Cancer Sci. 2010;101:2087–92. doi:10.1111/j.1349-7006.2010.01650.x.
19. Palchetti I. Affinity biosensors for tumor-marker analysis. Bioanalysis. 2014;6:3417–35. doi:10.4155/bio.14.247.
20. Labib M, Berezovski MV. Electrochemical sensing of microRNAs: avenues and paradigms. Biosens Bioelectron. 2015;68:83–94. doi:10.1016/j.bios.2014.12.026.
21. Campuzano S, Pedrero M, Pingarrón JM. Electrochemical genosensors for the detection of cancer-related miRNAs. Anal Bioanal Chem. 2013;406:27–33. doi:10.1007/s00216-013-7459-z.
22. Teo AKL, Le Lim C, Gao Z. The development of electrochemical assays for microRNAs. Electrochim Acta. 2014;126:19–30. doi:10.1016/j.electacta.2013.06.113.
23. Bartosik M, Hrstka R, Palecek E, Vojtesek B. Adsorptive transfer stripping for quick electrochemical determination of microRNAs in total RNA samples. Electroanalysis. 2014;26:2558–62. doi:10.1002/elan.201400449.
24. Torrente-Rodríguez RM, Campuzano S, López-Hernández E, Granados R, Sánchez-Puelles JM, Pingarrón JM. Direct determination of miR-21 in total RNA extracted from breast cancer samples using magnetosensing platforms and the p19 viral protein as detector bioreceptor. Electroanalysis. 2014;26:2080–7. doi:10.1002/elan.201400317.
25. Erdem A, Congur G. Label-free voltammetric detection of microRNAs at multi-channel screen printed array of electrodes comparison to graphite sensors. Talanta. 2014;118:7–13. doi:10.1016/j.talanta.2013.09.041.
26. Tran HV, Piro B, Reisberg S, Duc HT, Pham MC. Antibodies directed to RNA/DNA hybrids: an electrochemical immunosensor for microRNAs detection using graphene-composite electrodes. Anal Chem. 2013;85:8469–74. doi:10.1021/ac402154z.
27. Kilic T, Nur Topkaya S, Ozsoz M. A new insight into electrochemical microRNA detection: a molecular caliper, p19 protein. Biosens Bioelectron. 2013;48:165–71. doi:10.1016/j.bios.2013.04.011.
28. Baydemir G, Bettazzi F, Palchetti I, Voccia D. Strategies for the development of an electrochemical bioassay for TNF-alpha detection by using a non-immunoglobulin bioreceptor. Talanta. 2016;151:141–7. doi:10.1016/j.talanta.2016.01.021.
29. Laschi S, Palchetti I, Marrazza G, Mascini M. Development of disposable low density screen-printed electrode arrays for simultaneous electrochemical measurements of the hybridisation reaction. J Electroanal Chem. 2006;593:211–8. doi:10.1016/j.jelechem.2006.04.015.
30. Bettazzi F, Hamid-Asl E, Esposito C, Quintavalle C, Formisano N, Laschi S, et al. Electrochemical detection of miRNA-222 by use of a magnetic bead-based bioassay. Anal Bioanal Chem. 2013;405:1025–34. doi:10.1007/s00216-012-6476-7.
31. Laschi S, Bulukin E, Palchetti I, Cristea C, Mascini M. Disposable electrodes modified with multi-wall carbon nanotubes for biosensor applications. ITBM-RBM. 2008;29:202–7. doi:10.1016/j.rbmret.2007.11.002.
32. Hoogvliet JC, Dijksma M, Kamp B, van Bennekom WP. Electrochemical pretreatment of polycrystalline gold electrodes to produce a reproducible surface roughness for self-assembly: a study in phosphate buffer pH 7.4. Anal Chem. 2000;72:2016–21. doi:10.1021/ac991215y.
33. Findlay JWA, Dillard RF. Appropriate calibration curve fitting in ligand binding assays. AAPS J. 2007;9:E260–7. doi:10.1208/aapsj0902029.
34. Giannetto M, Maiolini E, Ferri EN, Girotti S, Mori G, Careri M. Competitive amperometric immunosensor based

on covalent linking of a protein conjugate to dendrimer-functionalised nanogold substrate for the determination of 2,4,6-trinitrotoluene. Anal Bioanal Chem. 2012;405:737–43. doi:10.1007/s00216-012-6137-x.
35. O'Mullane AP, Ippolito SJ, Sabri YM, Bansal V, Bhargava SK. Premonolayer oxidation of nanostructured gold: an important factor influencing electrocatalytic activity. Langmuir. 2009;25:3845–52. doi:10.1021/la8039016.
36. Hezard T, Fajerwerg K, Evrard D, Collière V, Behra P, Gros P. Gold nanoparticles electrodeposited on glassy carbon using cyclic voltammetry: application to Hg(II) trace analysis. J Electroanal Chem. 2012;664:46–52. doi:10.1016/j.jelechem.2011.10.014.
37. Komsiyska L, Staikov G. Electrocrystallization of Au nanoparticles on glassy carbon from HClO4 solution containing [AuCl4]−. Electrochim Acta. 2008;54:168–72. doi:10.1016/j.electacta.2008.08.013.
38. Zanardi C, Baldoli C, Licandro E, Terzi F, Seeber R. Development of a gold-nanostructured surface for amperometric genosensors. J Nanopart Res. 2012;14:1–12. doi:10.1007/s11051-012-1148-2.
39. Welch CM, Nekrassova O, Dai X, Hyde ME, Compton RG. Fabrication, characterisation and voltammetric studies of gold amalgam nanoparticle modified electrodes. ChemPhysChem. 2004;5:1405–10. doi:10.1002/cphc.200400263.
40. Bettazzi F, Lucarelli F, Palchetti I, Berti F, Marrazza G, Mascini M. Disposable electrochemical DNA-array for PCR amplified detection of hazelnut allergens in foodstuffs. Anal Chim Acta. 2008;614:93–102. doi:10.1016/j.aca.2008.03.027.

Diego Voccia is a post-doctoral researcher in analytical chemistry at the Department of Chemistry of the University of Florence.

Francesca Bettazzi is a post-doctoral researcher at the Department of Chemistry of the University of Florence. Her research interests are the development of electrochemical biosensors for the detection of clinically and environmentally relevant molecules.

Emiliano Fratini is Associate Professor at the University of Florence (Department of Chemistry) and member of CSGI. He received his Ph.D. in Chemistry in 2001 from the University of Florence. Since 2000, he has been carrying out experimental studies at MIT and NCNR (on hydration water in porous media and biomolecules, neutrons and x-rays characterization of soft matter). Currently he teaches classes in nanomaterials, materials chemistry, and physical chemistry of foods. His main research interests are on multifunctional nanocomposites, design of novel hydrogels and organogels, development of mesoporous silica scaffolds for catalysis and actives delivery, and structural and dynamical characterization of nanomaterials and soft matter.

Debora Berti is Associate Professor of Physical Chemistry at the Department of Chemistry of the University of Florence. She currently supervises a group working in the field of physical chemistry of soft matter for applications in the biomedical area. Her research topics include hybrid nanoparticle/lipid assemblies for responsive drug delivery, interaction of nanostructured assemblies with model membranes, and nanostructured fluids for the conservation of cultural heritage.

Ilaria Palchetti is an Associate Professor of Analytical Chemistry at the Department of Chemistry of the University of Florence (Italy). She received her Ph.D. in Environmental Science from the University of Florence (Italy). Her research interests include sensor and biosensor development, analytical chemistry, electrochemistry, photoelectrochemistry, and nanotechnologies for sensor production.